JOURNAL OF MATERIALS SCIENCE 7 (1972) 105–114

X-Ray Diffraction Study of Tensile Deformation in a Bulk Polycrystalline Ag-30 at. % Cd Alloy*

H. A. DAVIES†, C. N. J. WAGNER‡
Hammond Laboratory, Yale University, New Haven, Connecticut, USA

X-ray diffraction techniques have been used to study plastic deformation in a polycrystalline Ag-30 at.% Cd alloy under tensile load. The positions and shapes of all (hkl) reflections were recorded using a parafocusing arrangement up to a maximum true strain of 0.265. The effects on the peak displacements caused by stacking faults and by macroscopic strains normal to the surface were distinguished. The longitudinal true stress in the surface layer evaluated by least square analysis was smaller than the macroscopic flow stress by an approximately constant amount over the whole range of strain (in accord with previous observations of a stress gradient near a free surface); the apparent *rate* of work hardening in the surface was equal to that for the specimen as a whole. The stacking fault probability α was approximately a linear function of strain and attained a maximum value of 7×10^{-3}.

Fourier analyses were performed on the profiles of (111) – (222) and (200) – (400) pairs of reflections. The effective particle sizes $D_e(111)$ and $D_e(100)$ and the estimated true domain size D decreased approximately inversely with increasing strain, tending to limiting values at high strains of 220, 150 and 300 Å respectively. Similarly, the microscopic strains $[\langle \epsilon_L^2 \rangle_{hkl}^*]^{\frac{1}{2}}$ tended to limiting values at high mechanical strains. The twin fault concentration was found to be negligibly small. The particle size and microstrain parameters were compared with values for cold-worked filings of the alloy. A plot of α against $\langle \epsilon_L^2{}_{=50\text{Å}} \rangle_{111}^*$ for the solid specimens and for the filings was linear and yielded a stacking fault energy for Ag-30 at. % Cd of 6.1 ergs/cm^2.

1. Introduction

Analysis of the changes in the positions and shapes of X-ray powder pattern peaks provides a useful technique for studying quantitatively the microstructure and state of strain resulting from the plastic deformation of metallic materials [1-3]. Peak broadening may be caused by coherently diffracting domains less than 1000 Å diameter, non-uniform microstrains within these domains and deformation faults [1, 2]. Changes in the peak positions may be due to applied or residual macroscopic stresses, stacking faults [4] and, in certain cases, to changes in lattice parameter produced by the redistribution of solute atoms [5]. Twin faulting in crystallites also gives rise to asymmetry of peaks [3]. By careful measurement and analysis it is possible to separate quantitatively the microstrain and particle size contributions to the peak broadening and the macrostrain and stacking fault contributions to the peak displacement. Moreover, further analysis of the relationship between the derived faulting and microstrain parameters enabled an estimate of the stacking-fault energy of the material to be made [6].

Although much of the information obtained is indirect, X-ray techniques are a useful complement to electron microscopy in this field. They are non-destructive and are not subject to systematic errors which may result from the

*This work was supported by the Office of Naval Research
†Present Address: Department of Metallurgy, The University, Sheffield, UK
‡Present Address: Materials Department, University of California, Los Angeles, USA

chemical thinning of foils. Moreover, the volume of material sampled by an X-ray beam is many orders of magnitude greater than that observed in an elecron microscope and so there is a reduction in volume-dependent errors.

Most of the X-ray studies of deformed metals and alloys have concentrated either on the peak broadening or on the peak displacement and usually after unloading of the specimen. Moreover, much of the work in which a simultaneous determination was made of stress and change in structure was concerned with compressed powders [7-10] which are of limited practical importance, compared with bulk polycrystalline material. The majority of the X-ray measurements of stress have shown that the effective stress in the surface region penetrated by the radiation is lower than the average stress applied to the specimen [7, 8, 10-12] although, in some cases, only one or two reflections were used and some uncertainty existed about the appropriate values of planar elastic constants. There is experimental evidence, other than X-ray diffraction, to support the existence of a lower stress in the surface [13-15] but, on the other hand, it contradicts the interpretation placed on the results of other experiments, notably those of Kramer *et al* [16], where it was concluded that a hardened layer is present at the surface of deformed crystalline material.

The present work was undertaken in order to study:

(i) the changes in lattice parameter as a function of elongation of a specimen, *while it was under load and using all the available X-ray reflections*, in an attempt to resolve the controversy regarding the state of stress in the surface of deformed material.

(ii) the microstructural changes brought about by plastic deformation of a bulk polycrystalline alloy having a low stacking fault energy.

The Ag-30 at. % Cd alloy was chosen partly because it was known to have a low stacking-fault energy [5, 38] and partly because cadmium has approximately the same scattering power as silver, so that any asymmetrical effect on the diffraction profiles due to unequal scattering powers of the (1 1 1) faulting planes would be minimised [17]. This followed on a similar study made earlier in this laboratory no an Ag-9 at. % Sn alloy [18, 19] in which the analysis of the data was complicated by large decreases in the true lattice parameter, apparently due to solute segregation. It was expected, from experience with filings [5], that this effect would be largely avoided in this alloy. Bragg-Brentano focusing geometry was used in conjunction with flat tensile specimens, since this method gives less instrumental broadening than the non-focusing Debye-Scherrer geometry. Fourier analysis of line broadening was preferred to integral breadth analysis, since the former yields more detail of the microstrain distribution and no assumption is required about the shapes of the peaks.

2. Experimental Procedure

Ingots of the Ag-30 at. % Cd alloy were prepared by melting together 99.99% pure silver and cadmium in vacuum-sealed quartz tubes. These ingots were alternately cold-rolled and annealed to attain a thickness of 0.063 in. and flat tensile specimens, having gauge lengths of rectangular section (0.2 in. wide × 0.030 in. thick) and length 1.5 in., were machined from them. They were then given a final anneal at 400°C for 1 h resulting in a grain size of approximately 30 μm. Back-reflection photographs were taken to confirm that they were fully annealed.

The annealed specimen was mounted horizontally on to a miniature tensile machine (designed by Materials Research Corporation, Orangeburg, New York) [18]. Tension on the specimen was provided by the compression of a spring, which had been calibrated on an Instron tensile machine; compression of the spring and the change in length of the specimen were registered by means of dial gauges. The tensile machine was mounted on a G.E. XRD-5 diffractometer, so that the flat surface of the specimen was tangential to the focusing circle.

The specimen was deformed slowly up to a maximum of about 31% elongation, X-ray measurements being made at intervals of between 2 and 6% elongation. All available reflections from the silver alloy specimen (between (1 1 1) and (5 1 1) – (3 3 3)) were measured at 27°C with β-filtered CuKα radiation using a 3° divergence slit, a medium resolution Soller slit and 0.1° receiving slit. The line profiles of the annealed sample and the strong reflections of the cold-worked sample were recorded continuously using a ratemeter and recorder; a step-scanner and printer were used for the weak reflections. Careful attention was given to aligning the diffractometer and this was checked at alternate states of elongation by brushing a thin layer of annealed aluminium powder on to the specimen

surface and measuring the peak positions from all available reflections.

Separation of the Kα doublet was performed by the Rachinger method [3]. The accuracy of the peak maximum determination for the deformed specimen was about ± 0.02° in 2θ for low-angle peaks up to and including the (3 1 1) reflection and ± 0.05° for other peaks. The Fourier coefficients of all $K\alpha_1$ reflections from the deformed specimen were obtained by the Stokes method [3] using the annealed sample as a standard.

3. Analysis of the Diffraction Data

3.1. Peak Shifts due to Geometrical Factors, Stacking Faults and Macroscopic Stresses

For the focusing geometry of the diffractometer, the lattice parameter a_{hkl} of a specimen, in which a longitudinal macro-stress and stacking faults are present, is given by [3]:

$$a_{hkl} = a_0 + a_0\alpha G_{hkl} + a_0\epsilon_f J_{hkl} + a_0(S_1)_{hkl}\sigma + m\cos\theta\cot\theta \qquad (1)$$

where a_0 is the true lattice parameter; $\alpha = \alpha' - \alpha''$, where α' and α'' are the intrinsic and extrinsic stacking-fault probabilities; ϵ_f is the fractional change in lattice parameter at the faults; σ is longitudinal stress in the specimen; G_{hkl} and J_{hkl} [3] are constants dependent on the indices of the reflecting planes, $(S_1)_{hkl}$ is the elastic compliance for the (hkl) planes in a polycrystalline aggregate ($S_1 = -\nu/E$ where ν is Poisson's ratio and E is Young's modulus). The last term $m\cos\theta\cot\theta$ is a misalignment term where θ is the diffraction angle for the (hkl) planes and m is a constant dependent on the displacement of the sample from the focusing circle.

Several approximate methods for calculating the elastic compliances of polycrystalline aggregates from the single crystal elastic compliances s_{ij} have been proposed but the simplest approximation, which was used in the present work is to take the arithmetic mean of the extreme values given by the models of Voigt [20] and Reuss [21]. Markham [22] has shown that for a number of metals and alloys the mean value agreed to better than ± 2% with the experimental value (and with the value given by Kröner's model which was the most rigorous approach of all the models and which gave the best agreement with experiment).

Voigt assumed constant strain in the grains of the polycrystal, so that:

$$(S_1)^V = 2s_0(s_{11} + 2s_{12}) + 5s_{12}s_{44}/(6s_0 + 5s_{44})$$

Reuss assumed constant stress in all grains, so that:

$$(S_1)^R{}_{hkl} = s_{12} + s_0\Gamma$$

where

$$s_0 = s_{11} - s_{12} - \frac{s_{44}}{2}$$

and

$$\Gamma = (h^2k^2 + k^2l^2 + h^2l^2)/(h^2 + k^2 + l^2)$$

The s_{ij} for a number of silver-based alloys [37] were found to be approximately linear functions of valence-electron concentration e/a and those for the Ag − 30 at. % Cd alloy were obtained by linear extrapolation to $e/a = 1.3$. These and the derived value of $(S_1)^V$, $(S_1)^R{}_{hkl}$ and $(S_1)_{hkl} = [(S_1)^V + (S_1)^R{}_{hkl}]/2$ are given in table I.

For each state of strain of the tensile specimen the values of the five unknowns in equation 1, a_0, α, ϵ_f, σ and m were determined by setting up equations for all the available a_{hkl} (usually ten) and making a least squares analysis. (It was assumed that the scatter was due only to α, ϵ_f and σ).

The stress σ_A could also be estimated directly from the lattice parameter a_{app} obtained by extrapolating to $\cos\theta\cot\theta = 0$ a straight line through the points $(a_{111} + 2a_{200})/3$ and $(a_{331} + a_{420})/2$. If $(S_1)_A$ is the average of all $(S_1)_{hkl}$ (= − 0.524 × 10^{-12} cm²/dyne) then:

$$\frac{a_{app} - a_0}{a_0} = \sigma_A(S_1)_A \qquad (2)$$

At the highest strain imparted to the specimen, the stress was also determined independently by the commonly used "psi" method in which the specimen is rotated about the vertical axis of the diffractometer so that the X-rays are diffracted by planes not parallel to the surface, and the apparent change in the lattice parameter a_{hkl} measured as a function of angle ψ [23]. Elasticity theory gives:

$$\frac{a_\psi - a_\perp}{a_0} = (S_2/2)_{hkl} \cdot \sigma \cdot \sin^2\psi \qquad (3)$$

where a_ψ is the measured lattice parameter for hkl planes whose normal is at an angle ψ to the surface normal and $a_\perp$ is the lattice parameter measured for the hkl planes parallel to the surface. $(S_2/2)_{hkl} = (1 + \nu_{hkl})/E_{hkl}$.

A high angle reflection (4 2 2) was used for high

TABLE I Values of the constants G_{hkl}, J_{hkl}, $(S_1)_{hkl}^R$, $(S_1)^V$, $(S_1)_{hkl}$ and $(S_2/2)_{422}$ used in the evaluation of stresses and stacking fault probabilities in Ag-30 at.% Cd.

hkl	G_{hkl}	J_{hkl}	V_{hkl}	$-(S_1)^R$ ($\times 10^{12}$ cm^2/dyne)	$-(S_1)_{hkl}$ ($\times 10^{12}$ cm^2/dyne)	$(S_2/2)_{hkl}$ ($\times 10^{12}$ cm^2/dyne)
111	− 0.0345	0.209	0.43	0.245	0.320	
200	0.0689	− 0.167	1.00	1.19	0.792	
220	− 0.0341	− 0.167		0.481	0.438	
311	0.0125	0.038		0.745	0.570	
222	0.0172	0.209		0.245	0.320	
400	− 0.0345	− 0.167		1.19	0.792	
331	− 0.0073	− 0.167		0.413	0.404	
420	0.0069	0.234		0.737	0.555	
422	0	− 0.167		0.481	0.438	1.694
511 } 333 }	0.0029	− 0.010		0.805	0.600	

$-(S_1)^V = 0.395 \times 10^{12}$ cm^2/dyne
Single crystal elastic constants:
$S_{11} = 2.76 \times 10^{-12}$ cm^2/dyne
$S_{12} = 1.19 \times 10^{-12}$ cm^2/dyne
$S_{44} = 2.23 \times 10^{-12}$ cm^2/dyne

sensitivity and a_{422} measured at $\psi = 0°$, 23° and 40°. The receiving slit was set at a fixed optimum position for the range of ψ covered, since the position of the focal point of the diffracted beam is a function of ψ and, also, an absorption correction $\tan\psi \cot\theta$ was applied, prior to the determination of the maxima of the very broad (422) reflections.

3.2. Broadening of the Peaks

The profile $P_{2\theta}$ of a powder pattern peak, corrected for instrumental broadening, can be expressed as a Fourier series [1]:

$$P_{2\theta} \propto \sum_{L=-\infty}^{+\infty} \{A(L)\cos[4\pi L(\sin\theta - \sin\theta_0)/\lambda] + B(L)\sin[4\pi L(\sin\theta - \sin\theta_0)/\lambda]\}$$

where $A(L)$ and $B(L)$ are the sine and cosine coefficients, respectively, L is the distance normal to the reflecting planes, θ_0 is the position of the peak maximum and λ is the wavelength of the radiation. When θ_0 is taken as the origin of the Fourier transformation and when L, α and β (the twin-fault probability) are small, $A(L)$ can be expressed [2] as:

$$\ln A(L) = \ln A^P(L) - 2\pi^2(L^2/a_0^2)h_0^2(\langle\epsilon_L^2\rangle - \langle\epsilon_L\rangle^2)_{hkl} \quad (4)$$

The particle size term $A^P(L)$ is independent of the order of the reflection whereas the second term relating to the standard deviation of the microstrain distribution, $(\langle\epsilon_L^2\rangle - \langle\epsilon_L\rangle^2)_{hkl}^{\frac{1}{2}}$, is proportional to the square of the order $h_0^2 = h^2 + k^2 + l^2$. Hence, by plotting $\ln A(L)$ versus h_0^2 for two orders of reflections from the same planes, e.g. (111) and (222), the two contributions can be separated. This was performed for the ⟨100⟩ and ⟨111⟩ directions.

The effective particle sizes D_e (111) and D_e (100) given by the negative initial slopes of the $A(L)$ versus L plots can be expressed in terms of the true domain size D(hkl) and the stacking and twin-fault parameters α and β, thus:

$$1/D_e(111) = 1/D(111) + (\sqrt{3}/4a)(1.5\alpha + \beta) \quad \ldots\ldots (5)$$

$$1/D_e(100) = 1/D(100) + (1/a)(1.5\alpha + \beta) \quad (6)$$

Most of the calculations, including Rachinger separation of $K\alpha_1$ and $K\alpha_2$, determination of the positions of the peak maxima, solution of a_0, a_{app}, α, ϵ_f, σ and m from equation 1, Fourier analyses of the broadened peaks and Stokes correction for instrumental broadening, were performed using programmes written in Fortran for IBM 7094 and 360 computers.

4. Experimental Results

4.1. Lattice Parameters

Initially, the lattice parameters of annealed and cold-worked filings were measured for the purpose of comparison. The extrapolated lattice parameter of the as-filed material was found to be very slightly smaller (0.2%) than that of the annealed filings, possibly due to segregation of some solute atoms to stacking faults, since least squares analysis of the peak displacements indicated that no net residual macroscopic stress was present.

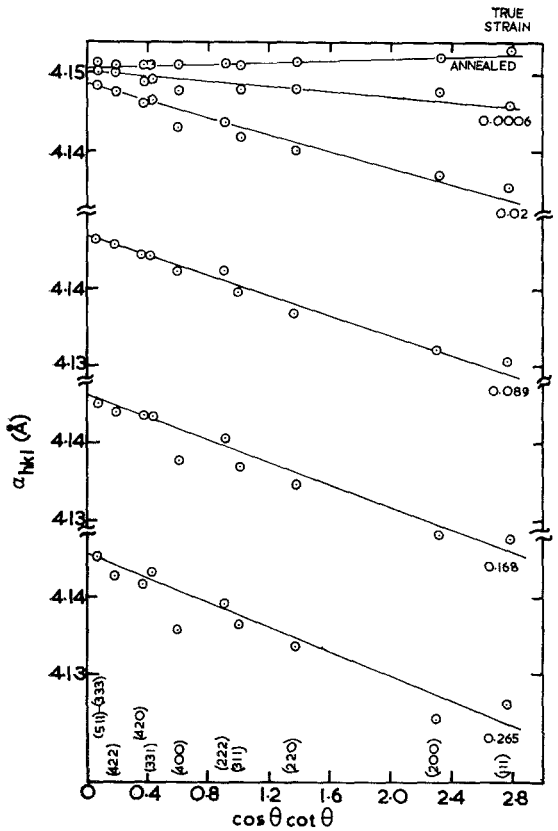

Figure 1 Lattice parameters a_{hkl} against $\cos\theta \cot\theta$ of bulk Ag-30 at.% Cd deformed in tension to various strains.

The lattice parameters a_{hkl} of the Ag-30 at.% Cd alloy in the initial annealed state and at various stages of the tensile deformation are plotted against $\cos\theta \cot\theta$ in fig. 1. The scatter of the points for the specimen in the deformed state reflects the combined effects of stacking faults and compressive lattice strain normal to the surface.

The tensile stresses computed by least squares analysis of the a_{hkl} data using equation 1 are plotted as a function of true strain in fig. 2. (The true tensile strain ϵ_{true} is related to the measured engineering strain ϵ_{eng} by $\epsilon_{true} = \ln(1 + \epsilon_{eng})$. Also shown in fig. 2 is the macroscopic true stress-true strain curve measured with the miniature tensile machine; this curve was essentially in agreement with a test performed on a similar annealed sample of this material with an Instron tensile testing machine. Allowing for the uncertainty of about $\pm$ 3 kg/mm^2, the computed X-ray stress-strain curve shows a long, linear work-hardening region typical of a low

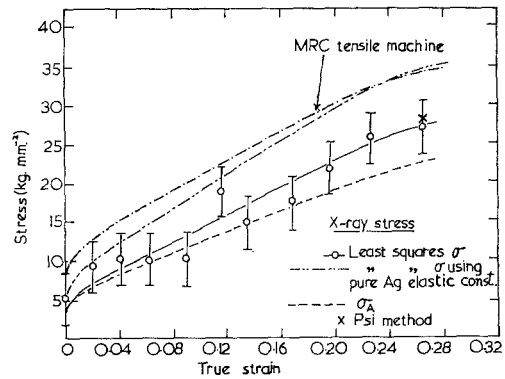

Figure 2 Comparison of computed X-ray surface stresses with the mechanical stress-strain curve for the tensile specimen.

stacking-fault energy material with a slope similar in magnitude to that observed in the mechanical test, but with the X-ray stress being lower than the applied stress by 6 to 7 kg/mm^2 over the whole range of strain.

The tensile stresses σ_A calculated from $a_{app} - a_0$ using equation 2 are summarised as the dashed curve in fig. 2; these are in good agreement with those given by the least squares analysis at strains up to 0.1 but are 10 to 15% lower at higher strains. The true lattice parameter a_0 decreased by up to 0.06% in the initial stages of the deformation but stabilised to a value, on average, about 0.02% below that for the annealed specimen, a_0^{ann}, as the deformation proceeded.

The lattice stress determined by the "psi" method for the highest strain, 28 kg/mm^2, compares favourably with the corresponding least squares σ, 27 kg/mm^2, and is again smaller than the mechanical stress by about double the uncertainty in the measurement.

The stacking-fault probability α increases progressively, and almost linearly, with increasing true strain as is shown in fig. 3. Values calculated by the method of slopes [24], also shown, are slightly lower. The maximum value of α achieved by the bulk specimen (0.007) is lower by a factor of 2.5 than the value for the cold-worked filings (0.018).

4.2. Fourier Analysis

The effective particle sizes D_e(hkl) in the $\langle 1\,1\,1 \rangle$ and $\langle 1\,0\,0 \rangle$ directions, obtained from the initial slope of the strain-corrected Fourier coefficients $A^P(L)$, are plotted against true strain in fig. 4.

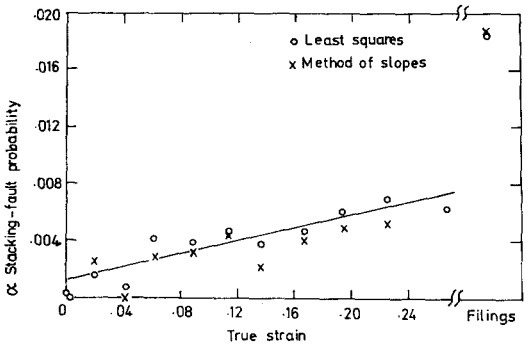

Figure 3 Stacking-fault probability α as a function of true strain for the bulk alloy. α for the cold-worked filings is also shown for comparison.

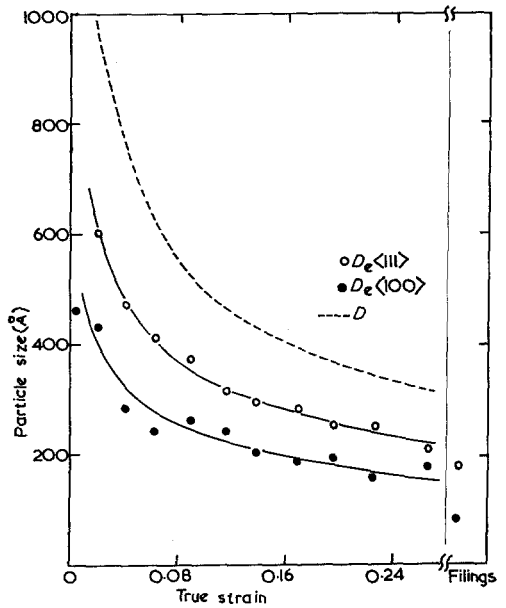

Figure 4 Effective particle sizes D_e (hkl) and the true domain size D as a function of true strain for the bulk specimen and for the cold-worked filings.

The results for the ⟨100⟩ direction at high strains are subject to greater uncertainty than those for the ⟨111⟩ direction since the (400) profile was very weak and diffuse. Indeed, it was observed that the (200) and (400) reflections were somewhat weaker and the (111) and (220) reflections somewhat stronger relatively than would be predicted for random powders which is consistent with a {110}⟨112⟩ texture [25] being introduced during the preparation by rolling of the specimen.

The D_e(hkl) are anisotropic and are approximately inversely proportional to the true strain, the diameter decreasing rapidly in the initial stage of straining but tending to level off as the deformation proceeds. This is similar to the observations of Otte and Adler [26] on α-brass and Wagner *et al* [8] on compressed copper sheet and filings. The ratio $D_e(111)/D_e(100)$ for the bulk specimen remained about 1.5 over the entire range of strain compared with the value of 1.95 observed for the filings.

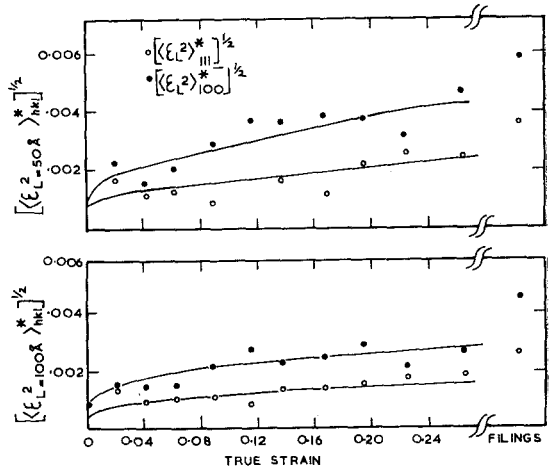

Figure 5 Standard deviation of the microstrain distribution $[\langle\epsilon_L^2\rangle_{hkl}^*]^{\frac{1}{2}}$ as a function of true strain for the bulk alloy and for the filings.

The standard deviation of the microstrains normal to the reflecting planes (which, henceforth, we shall denote by $[\langle\epsilon_L^2\rangle_{hkl}^*]^{\frac{1}{2}}$, calculated from the slopes of the $\ln A(L)$ versus h_0^2 plots (equation 4) decreased asymptotically with increasing L which, in effect, reflects the strain distribution around a dislocation. The variation of $[\langle\epsilon_L^2\rangle_{hkl}^*]^{\frac{1}{2}}$ with deformation for $L = 50$Å and $L = 100$Å in the ⟨111⟩ and ⟨100⟩ directions is shown in fig. 5; they increase fairly rapidly in the initial stages but level off as the deformation proceeds, in harmony with the changes in D_e(hkl). As for the D_e(hkl), they are anisotropic, $[\langle\epsilon_L\rangle_{100}^*]^{\frac{1}{2}}$ being approximately twice as great as $[\langle\epsilon_L^2\rangle^*_{111}]^{\frac{1}{2}}$. The shape of the plot of $[\langle\epsilon_L{}^{2=50\text{Å}}\rangle_{100}^*]^{\frac{1}{2}}$ against true strain bears a close resemblance to that of the derived X-ray flow curve in fig. 2.

Twin fault probabilities given by analysis of the asymmetry of the diffraction profiles were found to be negligibly small.

5. Discussion

5.1. X-Ray Stress Measurement

The longitudinal stress derived from the X-ray data by least squares analysis of the displacements of all the peaks is smaller than the true applied stress, i.e. the average macroscopic flow stress, by a constant amount which is a factor of two greater than the estimated uncertainty in the former. At the highest strain of 0.265, the stress given by the "psi" method, which should be independent of the effects of stacking faults for the (422) reflection, is an excellent agreement with the least squares calculation. As far as the present authors are aware, this represents the first attempt to compare these two methods of stress determination, although previous measurements utilising, independently, the "psi" method on nickel samples [11, 12] and least squares analysis on Ag-9 at. % Sn samples [18] have shown the surface longitudinal stresses to be considerably lower than applied stresses in specimens under tension. However, it is rather surprising to find that the rate of work hardening in the surface is similar to the average rate for the whole specimen.

Although the elastic constants for the present alloy are believed to be in error by not more than $\pm$ 2%, as a test, the least squares X-ray stresses were calculated using, in the extreme case, the single crystal elastic constants of pure silver. These are summarised as the double dashed line in fig. 2; the X-ray flow curve is now rather improbable since there is good agreement with the mechanical stress at high strains but poor agreement at low strains and resulting in a greater rate of work hardening in the surface.

The stresses σ_A calculated from $(a_{app} - a_0)$, in which the a_{app} were estimated from the positions of only four of the reflections, are less reliable than those calculated by least squares analysis. The stress-strain relationship given by this method is similar to that observed by Kolb and Macherauch [11] in which the difference between the X-ray and applied stress increases with increasing deformation, unlike the constant difference given by the least squares analysis.

In the work of Otte and his co-workers [24, 26] the X-ray stresses were determined by the method of equation 2. The X-ray stress-strain curves were fitted to the mechanical flow curves; for silicon bronze, good correspondence was obtained when the elastic compliances were chosen so that, instead of being the mean of Reuss and Voigt values, they were weighted 90 Voigt/10 Reuss. For α-brass, the weighting required for the best fit was 75 Voigt/25 Reuss. Clearly, since the Voigt elastic compliance is smaller than the average Reuss compliance in each case, a 50/50 weighting would have given smaller X-ray stresses, consistent with the present work. On unloading the α-brass specimens, residual tensile surface stresses were observed, in contradiction with previous observation of residual compressive surface stresses [11, 12, 23]. Stresses were calculated by Otte from the quantity $(a_{app} - a_0^{ann})$; if a_0 decreased with increasing deformation, as might be possible in alloys which fault profusely and as indeed happens, in the present case, the surface stresses would be overestimated and, in the extreme case, might result in the residual stresses appearing to be tensile. Experience with cold-worked α-brass filings [27] does not, however, lend support to a possible decrease in a_0.

The X-ray evidence appears then to be overwhelmingly in favour of a lower effective stress existing in the surface of deformed crystals than in their interior. Unfortunately, the X-ray studies of themselves do not provide much insight into the effective depth of this surface layer, in which the stress is lower than the average, except in so far as it is probably of the same order as the effective depth of penetration of the radiation (about 20 μm). Efforts have been made [28] to determine the surface stress in steel using radiation of different wavelengths, and thus having different degrees of penetration, but the results were somewhat inconclusive.

There is much experimental evidence to support the X-ray results. Kolb and Macherauch [11], during etching experiments in support of their X-ray study of nickel under tension, showed that the dislocation density was considerably smaller in the surface region than in a region 0.3 mm below and, subsequently [12], showed that the distribution of residual stress in a deformed specimen was inhomogeneous up to a depth of 150 μm below the surface. They concluded that the less severe work hardening in the surface resulted simply from the surface grains being under less constraint with regard to slip processes. The conclusions of the electron microscopic study of Swann [13] on deformed polycrystalline copper and the flow stress measurements and electron microscopy of Fourie [14, 29] on deformed single crystals of copper are also qualitatively in agreement with the present work. Fourie demonstrated that a soft region extended

TABLE II Engineering strain, true strain, true applied stress, lattice parameters a_{app} and a_0 and deformation fault probability ($1.5\alpha + \beta$) in Ag-30 at.% Cd, deformed in tension.

Eng. strain %	True strain	True applied stress (kg.mm^{-2})	a_{app} (Å)	a_0 (Å)	$\Delta a = a_{app} - a_0$ (Å) $\times 10^4$	$(1.5\alpha + \beta)$ ($\times 10^3$)
Ann.	0	0	4.15095	4.15095	0	
0.06	0.0006		4.1496	4.1510	14	
2.05	0.02	13.0	4.1482	4.1491	9	6.2
4.1	0.041	15.3	4.1472	4.1487	15	7.5
6.2	0.062	17.3	4.1467	4.1489	22	8.0
8.9	0.089	19.9	4.1468	4.1490	22	9.2
11.5	0.115	22.4	4.1457	4.1500	43	9.7
14.2	0.137	24.6	4.1476	4.1502	26	10.2
17.2	0.168	27.6	4.1462	4.1492	30	10.8
21.1	0.195	30.1	4.1472	4.1507	35	11.3
24.9	0.225	32.4	4.1460	4.1506	46	12.3
30.9	0.265	34.1	4.1455	4.1501	46	13.9

to a depth as great as 2 mm below the surface, at least in a single crystal, although in a polycrystalline material one would not expect the soft region to extend as far. Further support for the existence of a soft surface layer is provided by Brydges [15] and Block and Johnson [30]. The present observations and the supporting evidence cited above therefore contradict the interpretation placed by Kramer *et al* [16] on the experiments of Kitajima *et al* [31] in which it was concluded that a hardened layer is found at the surface of plastically deformed crystals.

5.2. Particle Sizes and Microscopic Strains

As shown in equations 5 and 6, the effective particle sizes D_e(hkl) are inversely proportional to α (when $1/D$ is either negligibly small or isotropic and a linear function of true strain ϵ) and since, by observation (fig. 3), α is directly proportional to ϵ, we expect D_e(hkl) to be proportional to ϵ^{-1}. This is found to be approximately the case for both the $\langle 100 \rangle$ and $\langle 111 \rangle$ directions, as shown in fig. 4.

If deformation faults are entirely responsible for the anisotropy of D_e(hkl), i.e. the true domain or cell size D is very large, then the theoretical ratio of $D_e(111)/D_e(100)$, given by equations 5 and 6, would be 2.3. Allowing for experimental uncertainty, this is seen to be the case for the filings where the ratio is 1.95. The lower ratios of about 1.5 for the bulk specimen suggest that one or more factors, in addition to the faulting, are contributing to the anisotropy. Values of D and of the compound fault probability ($1.5\alpha + \beta$) were calculated, assuming D to be isotropic. The values of D are plotted against true strain in fig. 4. The magnitude of D is realistic, tending to a limiting value of 300Å which is of the same order as the average distance between dislocations in a cold-worked lattice. The dependence of D on applied strain is similar to that of D_e(hkl).

Values of ($1.5\alpha + \beta$) for the tensile specimen are slightly larger than the corresponding values of 1.5α calculated from the peak displacement. This could be interpreted as indicating the presence of a small concentration of deformation twin faults but, since the analysis of diffraction profile asymmetries indicated negligible concentrations, the difference probably arises from a rolling texture (which was mentioned in section 4) so that the dislocation arrangement, and hence the true particle size, are anisotropic.

For the filings, the value of ($1.5\alpha + \beta$) is 0.048 compared with $1.5\alpha = 0.028$ calculated from peak shifts. The difference between these two, 0.020, can be attributed to twin faults and compares favourably with the value of twin fault probability, 0.025, calculated from peak asymmetry.

The evidence suggests then that, for this low stacking fault energy alloy, the dislocation arrangement in the tensile specimen, deformed at low rates of strain and having an initial texture, is very different from that in the filings, where the strain rate would have been extremely high. It would be of interest to compare the dislocation arrangement in filings and deformed specimens of a low stacking fault energy material using transmission electron microscopy. Some selected

filings might be thin enough to be examined directly in a 1 MeV electron microscope without incurring the disadvantage of chemical thinning.

The microscopic strains obtained by Fourier analysis were also anisotropic. If the micro-stresses were isotropic, then $[\langle\epsilon_L^2\rangle^*_{100}]^{\frac{1}{2}}/[\langle\epsilon_L^2\rangle_{111}{}^*]^{\frac{1}{2}}$ should $= E_{111}/E_{100} = 3.2$ (where E_{hkl} is Young's modulus). The observed ratio is about 2.0; this is close to midway between the extremes of isotropic strains and isotropic stresses, which accords with the model assumed here for polycrystalline deformation when calculating stresses from the lattice parameter shifts.

5.3. Stacking-Fault Probability and Stacking-Fault Energy

The stacking fault probability α, as determined from lattice parameter changes (equation 1) represents the difference between the intrinsic fault probability α' and the extrinsic fault probability α'', i.e. $\alpha = \alpha' - \alpha''$. On the other hand, the peak asymmetry yields the value which is a weighted sum of the extrinsic fault probability and the true twin fault probability β', i.e. $\alpha = 4.5\alpha'' + \beta'$ [32]. As mentioned previously, the values of β are negligibly small so that we may assume α'' to be zero. Therefore, we will consider $\alpha = \alpha'$, i.e. α represents the intrinsic fault probability.

The increase in α with increasing true strain, ϵ, shown in fig. 3, indicates that faults are being continuously generated during the work-hardening process, the faulted area being approximately a linear function of ϵ. The higher value of α in the cold-worked filings, compared with the tensile specimen, is a reflection of the much higher speed and severity of the deformation during the filing process; this not only introduces larger concentrations of dislocations but probably also gives non-equilibrium stacking fault widths significantly larger than those in the bulk specimen [33]. The values calculated by the method of slopes are slightly lower than the corresponding values computed from all the peak displacements probably owing to the fact that the displacements of second-order reflections, on which the method is heavily dependent, are usually somewhat smaller than those predicted by the Paterson theory.

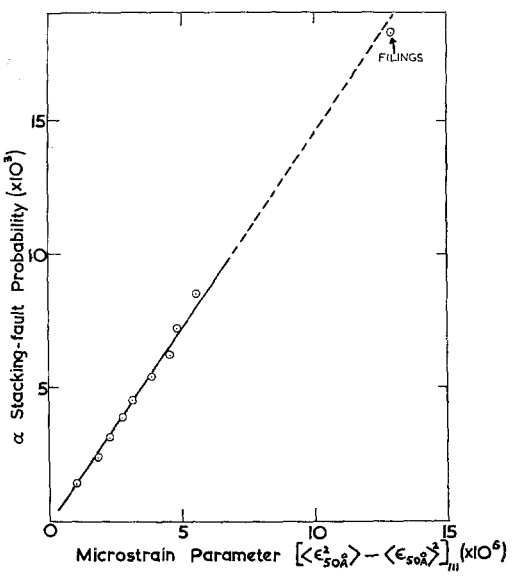

Figure 6 Stacking fault probability α as a function of micro-strain parameter $\langle\epsilon^2{}_{L=50\text{Å}}\rangle_{111}{}^*$.

It has been shown [6] that the stacking fault energy γ can be expressed in the following way:

$$\gamma = \frac{2E_{hkl}\, a_0}{\sqrt{3}\, F} \cdot \frac{\langle\epsilon_L{}^2{}_{=50\text{Å}}\rangle_{hkl}{}^*}{\alpha}$$

where E_{hkl} is the elastic modulus for the hkl lattice planes and F is a dimensionless factor which describes contributions to the stored energy of cold work due to single dislocations and to the interaction between dislocations. This factor has been estimated to equal about 5.0 for metals [34]. Therefore, a plot of α against $\langle\epsilon_L{}^2\rangle_{hkl}{}^*$ should be a straight line with a slope equal to $(2E_{hkl}\, a_0)_{hkl}/\sqrt{3\gamma F}$ from which γ can be calculated. The plot of interpolated values of α against $\langle\epsilon^2{}_{L=50\text{Å}}\rangle_{111}{}^*$ is shown in fig. 6; it approximates to a straight line with a slope of 1.47×10^3 and, rather surprisingly, in spite of the dislocation arrangement probably being markedly different, the point for the filings lies close to the extrapolation of the line passing through the points for the bulk specimen. Using a value of 9.4×10^{11} dyne/cm^2 for E_{111} (since $E = -\nu/S_1$ and $\nu \simeq 0.3$) we obtain a stacking fault energy of 6.1 ergs/cm^2 which compares favourably with a value of 5.1 ergs/cm^2 for Ag-29% Zn, estimated from the data of Howie and Swann [35] (and taking due account of the conversion factor of 2.3 for their data proposed by Brown [36]).

6. Summary

The broadening and displacement of X-ray diffraction peaks from a flat tensile specimen of Ag-30 at. % Cd have been studied while it was

deformed in a miniature tensile machine mounted on a diffractometer. The contributions to the displacement due to the longitudinal tensile stress and to the stacking faults were separated by least squares analysis and the broadening due to small effective particle sizes and high microstrains was Fourier analysed. The following conclusions were drawn:

(*a*) The calculated longitudinal tensile stress in the surface was significantly smaller than the true applied stress over the whole range of applied true strain ϵ. The difference was approximately constant so that the work-hardening rate in the surface was the same as that in the interior.

(*b*) The stacking-fault concentration α was approximately a linear function of ϵ, reaching a value of 0.007 at maximum ϵ of 0.265.

(*c*) The effective particle sizes $D_e(100)$ and $D_e(111)$ were approximately proportional to ϵ^{-1} and maintained a constant ratio $D_e(111)/D_e(100)$, of about 1.45. This suggested a contribution from a small true domain size D in addition to that from faulting. The derived values of D were also proportional to ϵ^{-1} and tended to a limiting value of about 300 Å.

(*d*) The standard deviation of the microstrain distribution $[\langle\epsilon_L^2\rangle - \langle\epsilon_L\rangle^2]^{\frac{1}{2}}$ tended to limiting values at high ϵ; for $L = 50$ Å in the $\langle 100\rangle$ direction the dependence of microstrain on ϵ was very similar to that of the calculated true stress.

(*e*) The stacking fault energy γ for Ag-30 at. % Cd was determined from the slope of a plot of α against $[\langle\epsilon_L^2\rangle_{111} - \langle\epsilon_L\rangle_{111}^2]$; this was linear for the whole range of ϵ and including the point for cold-worked filings of the same alloy and gave a value for γ of 6.1 ergs cm^{-2}.

Acknowledgement

The authors are grateful to Professor G. W. Greenwood for his comments on the manuscript.

References

1. B. E. WARREN, *Prog. Met. Phys.* **8** (1959) 147.
2. *Idem*, "X-ray Diffraction" (Addison Wesley, Reading Mass. 1969).
3. C. N. J. WAGNER, "Local Atomic Arrangement Studied by X-ray Diffraction" (ed. J. B. Cohen and J. E. Hilliard) (Gordon and Breach, New York, 1966) 219.
4. M. S. PATERSON, *J. Appl. Phys.* **23** (1952) 805.
5. R. P. I. ADLER and C. N. J. WAGNER, *ibid* **33** (1962) 3451.
6. R. P. I. ADLER, H. M. OTTE, and C. N.J. WAGNER, *Met. Trans.* **1** (1970) 2375.
7. K. KOLB and E. MACHERAUCH, *Z. Metalk.* **53** (1962) 108.
8. C. N. J. WAGNER, J. P. BOISSEAU, and E. N. AQUA, *Trans. Met. Soc. AIME* **233** (1965) 1280.
9. C. N. J. WAGNER, and J. HOEFL, *Trans. ASM* **60** (1967) 318.
10. C. J. NEWTON and A. W. RUFF, *J. Appl. Phys.* **37** (1966) 3860.
11. K. KOLB and E. MACHERAUCH, *Phil Mag.* **7** (1962) 415.
12. *Idem, Z. Metalk.* **53** (1962) 580.
13. P. R. SWANN, *Acta Metallurgica.* **14** (1966) 900.
14. J. T. FOURIE, *Phil. Mag.* **21** (1970) 173.
15. W. T. BRYDGES, *Scripta Metall.* **2** (1968) 557; *ibid* **3** (1969) 271.
16. I. R. KRAMER and A. KUMAR, *ibid* **3** (1969) 205.
17. B. T. M. WILLIS, *Acta Cryst.* **12** (1959) 683.
18. R. P. I. ADLER, D. Eng. Thesis, Yale University (1965).
19. R. P. I. ADLER and C. N. J. WAGNER, to be published
20. W. VOIGT, "Lehrbuch der Kristallphysik" (Teubner, Leipzig, 1928).
21. A. REUSS, *Z. Angew. Math. U. Mech.* **9** (1929) 49.
22. M. F. MARKHAM, *Mater. Res.* **1** (1962) 107.
23. G. B. GREENOUGH, *Prog. Met. Phys.* **3** (1952) 176.
24. H. M. OTTE and D. O. WELCH, *Phil. Mag.* **9** (1964) 299.
25. I. L. DILLAMORE, R. E. SMALLMAN, and W. T. ROBERTS, *ibid* **9** (1964) 517.
26. H. M. OTTE and R. P. I. ADLER, *Trans. Met. Soc. AIME* **239** (1967) 1092; *Phil. Mag.* **12** (1967) 239.
27. C. N. J. WAGNER and J. C. HELION, *J. Appl. Phys.* **36** (1965) 2830.
28. H. HENDUS and C. N. J. WAGNER, *Arch. Eisenhuttenw.* **8** (1955) 455.
29. J. T. FOURIE, *Phil. Mag.* **13** (1968) 735.
30. R. J. BLOCK and R. M. JOHNSON, *Scripta Metall.* **3** (1969) 511.
31. S. KITAJIMA, H. TANAKA, and H. KAIEDA, *Trans. J.I.M.* **10** (1969) 10.
32. B. E. WARREN, *J. Appl. Phys.* **34** (1963) 1973.
33. P. C. J. GALLAGHER and Y. C. LIU, *Acta Metallurgica* **17** (1969) 127.
34. R. P. I. ADLER and H. M. OTTE, *Mat. Sci. Eng.* **1** (1966) 222.
35. A. HOWIE and P. R. SWANN, *Phil. Mag.* **6** (1961) 1215.
36. L. M. BROWN, *ibid* **10** (1964) 441.
37. R. F. S. HEARMON, *Adv. Phys.* **5** (1956) 323.
38. R. G. DAVIES and R. W. CAHN, *Acta Metallurgica* **10** (1962) 621.

Received 27 July and accepted 10 August 1971.